J. Phys. B: At. Mol. Opt. Phys. **41** (2008) 105101 (8pp) doi:10.1088/0953-4075/41/10/105101

Photoionization of C_{60}: a model study

Mohamed E Madjet[1], Himadri S Chakraborty[2], Jan M Rost[3] and Steven T Manson[4]

[1] Freie Universität, Institut für Chemie (Kristallographie), Takustrasse 6, D-14195 Berlin, Germany
[2] Department of Chemistry and Physics, Northwest Missouri State University, Maryville, MO 64468, USA
[3] Max-Planck-Institut für Physik Komplexer Systeme, Nöthnitzer Strasse 38, D-01187 Dresden, Germany
[4] Department of Physics and Astronomy, Georgia State University, Atlanta, GA 30303, USA

E-mail: himadri@nwmissouri.edu

Received 2 March 2008, in final form 3 March 2008
Published 6 May 2008
Online at stacks.iop.org/JPhysB/41/105101

Abstract
Time-dependent density functional theory is used to calculate the total and subshell photoionization cross sections of C_{60}. The core of 60 C^{4+} ions is smeared into a classical jellium shell before treating the correlated motion of the 240 valence electrons quantum mechanically. The calculation reveals two collective plasmon resonances in the total cross section in agreement with the experiment. It is found that a *phase-coherent* superposition of amplitudes leading to enhancements in the ionization from various C_{60} subshells in two distinct energy regions essentially builds the plasmons. While the result shows good qualitative agreement with the experiments, the limitation of the model to describe the data in quantitative detail is discussed.

(Some figures in this article are in colour only in the electronic version)

1. Introduction

In atomic processes many intriguing phenomena observed in experiments are due to correlated electron motion. For surfaces and bulk matter, i.e., essentially infinitely extended objects, electron correlations induce collective phenomena, which are described in terms of plasmons or other 'quasi-particles'. For large finite systems such as clusters, one type of plasmon excitation can be classically visualized as a surface resonance where the negative charge density (delocalized electrons) oscillates as an incompressible fluid against the positive background density (ions). The dipole frequency ω_s of this surface oscillator is related to the characteristic plasma frequency ω_0 by $\omega_s = \omega_0/\sqrt{3}$. Using ultraviolet spectroscopy, a giant surface-plasmon was first observed at about 20 eV photon energy for gas phase C_{60} [1]. This measurement coincided with a theoretical prediction [2] that described the carbon core structure in a tight-binding model [3] and the response of C_{60} to an external electromagnetic field by the random-phase approximation. Accounting for the truncated icosahedron structure of the core in some approximate way other theoretical studies were also reported [4, 5].

Almost simultaneously, a different class of calculations of the photoionization of C_{60} has emerged where 60 C^{4+} ions are represented by a classical jellium shell [6–8]. The jellium model of the ion core disregards the motion of the 120 very tightly bound 1s electrons and treats the dynamics of the remaining 240 delocalized valence electrons self-consistently. This model gives rise to a single-electron ground-state potential having distinct edges at the positions of inner and outer radii of C_{60} and a nearly flat interior. Since free electrons (or quasi-free electrons in the interior of the potential) cannot absorb photons, the photoelectrons are created at the edges of the potential; this can be inferred from the form of the dipole matrix element known as 'acceleration gauge' which involves $\mathrm{d}V/\mathrm{d}r$ where V is the potential energy. The localized creation of electron waves produces path differences which lead to interferences in the photoionization cross section. More specifically, as a consequence of the geometry of the potential, the theory has predicted that the photoionization cross section should contain four oscillation frequencies [9]. Initially, three of them were identified in the measurement of photoionization cross sections of two outer valence orbitals of C_{60} which are in very good agreement with the jellium-based calculation [10]. The fourth one, which provides information about the thickness of the electron hull, was seen in a subsequent experiment [11].

Over the last few years a different kind of modelling of the C_{60} core has been established where the jellium approximation is only applied to 60 bare carbon nuclei, instead of 60 C^{4+}. The field due to the 120 1s electrons is calculated self-consistently by using the Hartree–Fock 1s atomic orbitals [12, 13]. The ground-state radial potential in this approach produces a cusp-shaped bottom. While calculations using such a cusp-bottom potential may produce good total photoabsorption cross sections, they predict only a single oscillation frequency in the photo cross section corresponding to the position of the cusp. Hence, they are inadequate to explain the experimental photoionization data [10] that contain multiple frequencies as mentioned above.

Going beyond these geometrical effects, which are single electron in nature, the description of plasmon resonances in C_{60} requires inclusion of many-body effects through electron correlation. Two practically equivalent approaches to include the correlation are (i) the random-phase approximation (RPA) and (ii) the time-dependent local density approximation (TDLDA). Both types of calculations have revealed the surface plasmon resonance [2, 6, 12, 13]. In addition, our recent calculation using the jellium-based TDLDA approach for singly ionized C_{60} has revealed the existence of a second collective resonance at a higher energy in agreement with the simultaneous experimental detection of this resonance [8]. While there is some discussion on the exact nature of this high-energy resonance [14], from the underlying asymmetric (compressional) mode of vibration of the electron cloud and from the proximity of this resonance frequency to the plasma frequency of the system, we called this feature a volume-like plasmon [15], being well aware of the fact that a volume plasmon in the strict sense cannot be excited by a dipole perturbation.

In an experiment on photoionization of the neutral C_{60} a similar high-energy resonance feature at about 40 eV photon energy [16] was observed, indicating that the occurrence of a high-energy plasmon is most likely generic in the photoionization of any fullerene system. Therefore, an effort to gain a detailed theoretical understanding to develop better insights of the collective behaviour that affects the photo response properties of these systems of hollow geometry is well motivated. In this paper, we describe in detail our calculations and present results for the photoionization of neutral C_{60}. For a better grasp on the underlying mechanism, the cross sections for independent subshells are also presented and it is shown how the cumulative superposition of various subshell cross sections builds up the plasmon resonances. The results are compared with measurements where available.

2. Details of the method

2.1. The jellium model

The jellium potential representing 60 C^{4+} ions is constructed as a uniform charge density over a spherical shell with radius R and thickness Δ. A constant pseudopotential V_0 is added [6]. R is taken to be the known radius of C_{60}, 3.54 Å. The Kohn–Sham equations for a system of 240 electrons are solved

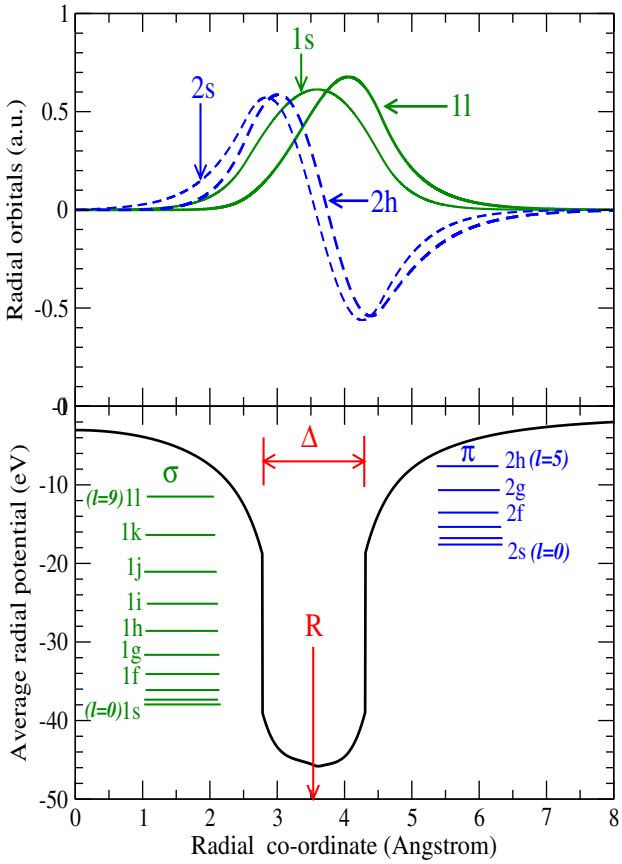

Figure 1. Top panel: LDA ground-state radial wavefunctions for the highest and the lowest ℓ of $n = 1$ (σ) and $n = 2$ (π) families. Bottom panel: radial potential averaged over orbital-specific potentials (see the text), and occupied π and σ level energies.

to obtain the single-electron ground-state orbitals in the local density approximation (LDA), and the parameters V_0 and Δ are determined by requiring both charge neutrality and obtaining the experimental value, 7.54 eV, of the first C_{60} ionization potential. This procedure yields a value of Δ of 1.5 Å, in excellent agreement with the value inferred from the experiment [10].

In addition, we include an appropriate correction to eliminate unphysical electron self-interactions for the ith subshell that renders the LDA potential orbital-specific [17, 18],

$$V^i(\mathbf{r}) = V_{\rm jel}(\mathbf{r}) + \int d\mathbf{r}' \frac{\rho(\mathbf{r}') - \rho_i(\mathbf{r}')}{\mathbf{r} - \mathbf{r}'} + (V_{\rm XC}[\rho(\mathbf{r})] - V_{\rm XC}[\rho_i(\mathbf{r})]), \quad (1)$$

where the terms on the right-hand side of the equation are, respectively, the jellium-electron, direct and exchange-correlation potentials. As the exact form of $V_{\rm XC}$ is unknown in a local formalism like LDA (since the exact exchange interaction is non-local), we employ a widely used parametric formulation [19]. In the bottom panel of figure 1 we show the radial potential 'averaged' over all the subshells. We stress that this potential with the two edges corresponding to the inner and outer radii, and a nearly flat bottom is quite

physical. This has become obvious from the role that it plays for the interpretation of the multiple frequencies in the Fourier transform of the measured photoelectron data [10].

In the bottom panel of figure 1 the ground-state energy levels for $n = 1$ (σ), $n = 2$ (π) groups are also shown. This conforms to the electron-momentum spectroscopic determination of C_{60}'s electronic structure being composed of a π and σ band [20]. Our approach is akin to [6] but for a crucial exception; in the ground-state configuration (in the harmonic oscillator nomenclature) $1s^2 1p^6 1d^{10} 1f^{14} 1g^{18} 1h^{22} 1i^{26} 1j^{30} 2s^2 2p^6$ $1k^{34} 2d^{10} 2f^{14} 1l^{18} 2g^{18} 2h^{10}$ we keep the 1 l subshell almost half-empty by filling it with only 18 electrons. This is done to ensure that two important properties of the system: (i) the two highest occupied molecular orbitals, HOMO and HOMO-1, are of 2 h and 2 g characters, respectively—a result well known from the quantum chemical calculations [21] supported by photoemission and inverse photoemission spectra [22], and from energy-resolved electron-momentum density measurements [20]; and (ii) the HOMO level is about half-filled—a consequence of the fact that the real system is slightly non-spherical, splitting some σ and π levels of higher angular momentum resulting in partially occupied 1 l and 2 h levels [4, 23]. It is remarkable that as a consequence of this artificial manipulation in a frame limited by the spherical geometry, our calculated ratio of HOMO and HOMO-1 cross sections, which is predominantly determined by the occupancy ratio of 2 h and 2 g levels ($10/18 = 0.56$), agrees so well with the experiment on an absolute scale [10].

Note in the top panel of figure 1 that, owing to strong electronic delocalization, both $n = 1$ (σ_ℓ) and $n = 2$ (π_ℓ) radial wavefunctions roughly occupy the same radial region, where ℓ denotes the orbital angular momentum with respect to the centre of C_{60}. π wavefunctions have one radial node, as opposed to the nodeless σ wavefunctions. In addition, all radial wavefunctions of π symmetry are nearly the same, independent of ℓ, and the same is true for the σ orbitals; this is in contrast to the situation in atoms where the radial wavefunctions of $n\ell$ orbitals with different ℓ are very different. As an indicator of the accuracy of the wavefunctions, the calculated static dipole polarizability of the system is 92.84 Å^3, which is reasonably close to the measured value 76.5 ± 8.0 Å^3 [24].

2.2. Dynamical response

A time-dependent LDA (TDLDA) approach [25–27] is used to calculate the dynamical response of the molecule to the external dipole field z. Since the molecule is rotationally invariant, Green's function for a parameter E can be expanded in the spherical basis:

$$G(\mathbf{r}, \mathbf{r}'; E) = \sum_{lm} G_{lm}(r, r'; E) Y^*_{lm}(\Omega) Y_{lm}(\Omega'), \tag{2}$$

where the radial component $G_{lm}(r, r'; E)$ satisfies the radial equation

$$\left(\frac{1}{r^2}\frac{\partial}{\partial r} r^2 \frac{\partial}{\partial r} - \frac{\ell(\ell+1)}{r^2} - V_{\mathrm{LDA}} + E\right) G_{lm}(r, r'; E) = \frac{\delta(r - r')}{r^2}. \tag{3}$$

G_{lm} is constructed with homogeneous solutions $j_l(r; E)$ and $h_l(r; E)$ of equation (3), satisfying boundary conditions at $r = 0$ and $r = \infty$ respectively, as

$$G_{lm}(r, r'; E) = \frac{j_l(r_<; E) h_l(r_>; E)}{W[j_l, h_l]}, \tag{4}$$

where the Wronskian

$$W[j, h] = r^2[j(r)\, \mathrm{d}h(r)/\mathrm{d}r - \mathrm{d}j(r)/\mathrm{d}r\, h(r)]_{r=c} \tag{5}$$

and is independent of the arbitrary constant c. Using Green's function, the independent particle (IP) susceptibility is then constructed by the ground-state single-electron orbitals ϕ_i and energies ϵ_i as

$$\chi_0(\mathbf{r}, \mathbf{r}'; \omega) = \sum_i \phi_i^*(\mathbf{r}) \phi_i(\mathbf{r}') G(\mathbf{r}, \mathbf{r}'; \epsilon_i + \hbar\omega) + \sum_i \phi_i(\mathbf{r}) \phi_i^*(\mathbf{r}') G^*(\mathbf{r}, \mathbf{r}'; \epsilon_i - \hbar\omega), \tag{6}$$

where the index i runs over the occupied states only.

The external perturbation z representing the dipole interaction of electrons with the linearly polarized light, induces a frequency-dependent complex change in the electron density. This can, in principle, be written as

$$\delta\rho(\mathbf{r}; \omega) = \int \chi(\mathbf{r}, \mathbf{r}'; \omega) z'\, \mathrm{d}\mathbf{r}', \tag{7}$$

where the full susceptibility χ incorporates the dynamical electron correlation. Using instead the IP susceptibility (equation (6)), the induced density can, equivalently, be written as

$$\delta\rho(\mathbf{r}; \omega) = \int \chi_0(\mathbf{r}, \mathbf{r}'; \omega) \delta V(\mathbf{r}'; \omega)\, \mathrm{d}\mathbf{r}', \tag{8}$$

in which

$$\delta V(\mathbf{r}'; \omega) = z + \int \frac{\delta\rho(\mathbf{r}'; \omega)}{|\mathbf{r} - \mathbf{r}'|}\, \mathrm{d}\mathbf{r}' + \left[\frac{\partial V_{\mathrm{xc}}}{\partial\rho}\right]_{\rho=\rho_0} \delta\rho(\mathbf{r}; \omega), \tag{9}$$

where the second and third terms on the right-hand side are, respectively, the induced change of the Coulomb and the exchange-correlation potentials. Obviously, besides including the external perturbation z, δV incorporates the dynamical field produced through many-electron interactions and, thereby, plays the role of an effective perturbation to the molecule.

χ is related to χ_0 by the matrix equation

$$\chi = \chi_0 \left[1 - \frac{\partial V}{\partial\rho} \chi_0\right]^{-1}, \tag{10}$$

involving the variation of the ground-state potential V with respect to the ground-state density ρ. Equation (10) can be solved for χ using the matrix inversion method [28]. $\delta\rho$ and, hence, δV can then be directly obtained via equations (7) and (9), respectively. Using the golden rule the photoabsorption cross section σ_{PA} is finally evaluated from the imaginary part of the polarizability α, and thereby, of $\delta\rho$ as

$$\sigma_{\mathrm{PA}}(\omega) = \frac{4\pi\omega}{c} \mathrm{Im}[\alpha(\omega)] = \frac{8\pi\omega}{c\mathcal{E}} \int z\, \mathrm{Im}[\delta\rho(\mathbf{r}; \omega)]\, \mathrm{d}\mathbf{r}', \tag{11}$$

where $\mathcal{E}$ is the magnitude of the external electric field.

It is also simple to derive an equivalent expression for the cross section in terms of δV directly as

$$\sigma_{\rm PA}(\omega) = 4\pi^2\gamma\omega \sum_{i,j} f_i(1-f_j)|\langle j|\delta V(\mathbf{r}';\omega)|i\rangle|^2 \times \delta(\hbar\omega - \epsilon_j + \epsilon_i), \quad (12)$$

where $\delta V(\mathbf{r}';\omega) = \delta V(r';\omega)Y_{10}(\Omega)$ to validate the dipole selection and f_i are Fermi occupation factors. Clearly, the index j scans the complete set of the single-electron excited as well as continuum states. Setting i to an occupied bound state $(n\ell)$ and j to the allowed continuum states $(k\ell')$, one can derive a formal expression for the photoionization cross section as the sum of the independent subshell cross sections $\sigma_{n\ell\to k\ell'}$, corresponding to a dipole transition $n\ell \to k\ell'$,

$$\sigma_{\rm PI}(\omega) = \sum_{n\ell}\sigma_{n\ell\to k\ell'} \sim \sum_{n\ell} 2(2\ell+1)|\langle\phi_{k\ell'}|\delta V|\phi_{n\ell}\rangle|^2. \quad (13)$$

The radial component $P_{k\ell}$ of the final continuum wavefunction $\phi_{k\ell}$ has the appropriate asymptotic behaviour:

$$\lim_{r\to\infty} P_{k\ell}(r) \sim \lim_{r\to\infty}[\cos(\delta_\ell)F_\ell(kr) + \sin(\delta_\ell)G_\ell(kr)] = \sin\left(kr - \frac{1}{2}\pi + \frac{z}{k}\ln(2kr) + \zeta_\ell + \delta_\ell\right) \quad (14)$$

where F_ℓ and G_ℓ are respectively the regular and irregular spherical Coulomb functions, and $\zeta_\ell = \arg\Gamma(\ell+1-{\rm i}z/k)$ is the Coulomb phase shift associated with the asymptotic charge z seen by the ejected electron.

Obviously, if we insert the result $\delta\rho_0$ (obtained either replacing χ by χ_0 in equation (7) or, equivalently, δV by z in equation (8)) in equation (11), we find the independent particle (IP) LDA result of the absorption cross section. Similarly, replacing δV in equation (13) by z yields the IP ionization cross section.

3. Results and discussion

3.1. Total cross section

The total photoionization cross section calculated in the TDLDA is presented in figure 2 as a function of the photon energy and is compared with the corresponding results from the LDA calculation that omits electron correlations. The comparison shows two regions of enhancement, plasmon resonances, in the TDLDA cross section. The low-energy resonance, that peaks at 16.5 eV, is seen to be also infested by a host of single-electron autoionizing resonances. This plasmon structure is the well-known giant dipole surface plasmon resonance. At 38.0 eV energy the second resonant structure emerges. This is expected given the recent experiment–theory joint study on C_{60} ions [8] and the determination of the feature in the experiment directly on neutral C_{60} [16]. Unlike the 16.5 eV resonance this structure exhibits a far weaker effect of single-electron resonances but a rather long decay range extending up to about 90 eV. Note that the enhancement caused by each of the resonances from the corresponding LDA result is roughly about an order of magnitude at their respective peaks. Furthermore, the calculation shows that the 16.5 eV and 38.0 eV plasmon resonances account for the

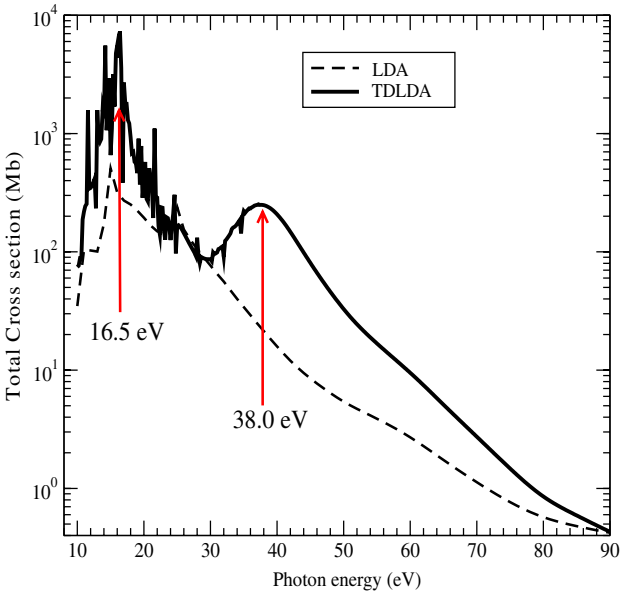

Figure 2. Total photoionization cross sections of C_{60} calculated in the LDA and TDLDA. The TDLDA result shows plasmon resonances at 16.5 eV and 38 eV photon energies.

oscillator strengths of about 130 and 30, respectively. Since the total oscillator strength for the photoabsorption process is the number of electrons (240 in this case) [29], this means that two-thirds of the total strength of the C_{60} photoabsorption process over the full range from the lowest discrete excitation to infinite energy is contained in the two collective plasmon resonances.

The emergence of plasmon resonances can be thought of as originating from the formation of collective states under the influence of the external electromagnetic field. A good way to visualize the mechanism is to consider explicitly, in terms of many-body ground $|\Phi_0\rangle$ and excited collective $|\Phi_m\rangle$ states, the complex polarizability α, that results from electrons' dipole interactions with the photon [26],

$$\alpha(\omega) = -\sum_m \left[\frac{|\langle\Phi_m|\zeta|\Phi_0\rangle|^2}{\hbar\omega - \Delta_m + {\rm i}\delta} - \frac{|\langle\Phi_m|\zeta|\Phi_0\rangle|^2}{\hbar\omega + \Delta_m + {\rm i}\delta}\right], \quad (15)$$

where $\zeta = \sum_i z_i$ are dipole interactions, $\Delta_m = E_m - E_0$ are many-body excitation energies and δ is an infinitesimal positive quantity. To a good approximation, $|\Phi_0\rangle$ can be constructed as a linear combination of Slater determinants of single-electron ground state ϕ_i's. Combining equation (15) with equation (11), the absorption cross section can be expressed as

$$\sigma_{\rm PA}(\omega) = \frac{4\pi\omega}{c}\delta\sum_m\left[\frac{|\langle\Phi_m|\zeta|\Phi_0\rangle|^2}{[\hbar\omega - \Delta_m]^2 + \delta^2} - \frac{|\langle\Phi_m|\zeta|\Phi_0\rangle|^2}{[\hbar\omega + \Delta_m]^2 + \delta^2}\right]. \quad (16)$$

The above expression suggests that the formation of resonance structures in the cross section at the photon energy Δ_m is due to excitations of the ground state Φ_0 to all possible collective excited states Φ_m that the system can support.

Theoretical studies of the dipole photoionization of solid spheres, such as metal clusters, predicted one plasmon resonance, indicating effectively one allowed collective excited state and, therefore, a single collective excitation [25, 30]. For large enough solid spheres another structure at a higher energy has also been predicted, but it is found to be far weaker than the main resonance and is suspected to originate from a non-local quantum-specific effect [25]. Moving from a solid sphere to a hollow shell, the geometry alters significantly. One direct effect of this change is an alteration in the distribution of ground-state single-electron energy levels (figure 1). This happens for the following reason: the hollow C_{60} geometry enables the electrons to move inside a spherical shell far from the molecular centre (large r), causing considerable weakening of the centrifugal barrier potential $\ell(\ell+1)/r^2$. Simultaneously, the narrower radial well of C_{60} compared to the relatively wide well of a solid system considerably separates the $n = 1$ and $n = 2$ radial levels. As a result, all ℓ levels for a given n tend to cluster, thereby inducing considerable separation between π and σ families in the ground-state spectrum of C_{60} (as seen in figure 1). In contrast, for a solid sphere a far broader radial potential and associated smaller values of r cause all single electron levels to mix together instead. It is therefore expected that this change in geometry from solid to shell also influences the formation of collective excited states of the respective systems. The hollow geometry allows for two many-body excited states, as opposed to one for the solid geometry. Therefore, in contrast to a metal cluster case, the photoionization cross section of C_{60} exhibits two plasmon resonances corresponding to the two collective excited states with excitation energies of about 16.5 eV and 38 eV. In the semi-classical interpretation of plasmon these two states can be identified with the symmetric and asymmetric eigenmodes of vibration of a classical dielectric shell [31].

3.2. Subshell cross sections

Since the collective excitations are embedded in the single-electron ionization channels, they provide alternative ionization channels degenerate with single-electron channels. Thus, the *autoionization* of these collective excited states induce resonance structures in the subshell cross sections. The cross sections for four outer π subshells, 2 h, 2 g, 2 f and 2 d, are presented in the top panel of figure 3. Both TDLDA and LDA results are shown for comparison purposes. All the TDLDA curves feature the low-energy resonance with the peak position being *exactly* at 16.5 eV, while the LDA curves at this energy region are seen to be practically flat. The spectral appearance of the resonance at rather the same energy in all subshell cross sections is expected since it is the same collective excitation which is degenerate with all energetically accessible π ionization continua. It may be noted that the 2 h cross section, in both the LDA and TDLDA, is somewhat weaker than the others in this energy region. This is simply because 2 h being partially filled with only 10 electrons provides fewer oscillators compared to the other completely filled subshells.

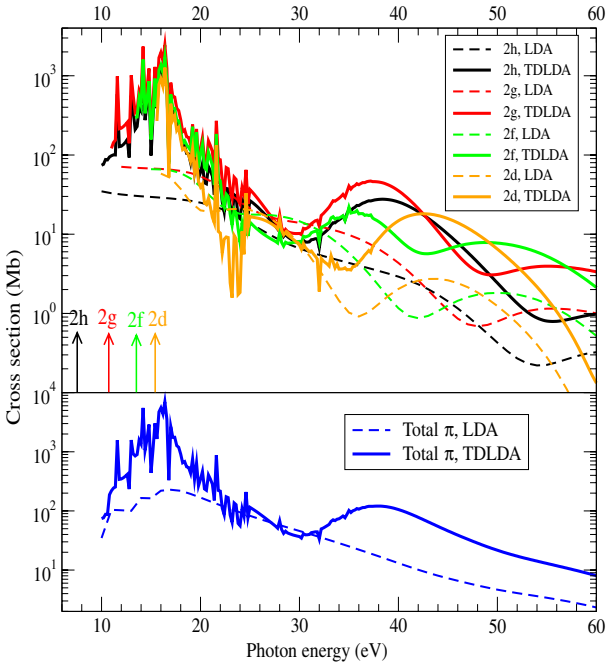

Figure 3. Upper panel: LDA and TDLDA cross sections for the four outer π subshells of C_{60}. The ionization thresholds of the subshells are also indicated. Lower panel: LDA and TDLDA total cross sections for all π electrons.

Beyond 30 eV, the geometry-dependent quantum interference (confinement) oscillations appear both in LDA and TDLDA curves for all the subshells, although the TDLDA cross sections are larger. It is, however, easy to see that these confinement oscillations are not at all in phase from one subshell to another. In fact, it was shown that in the high-energy limit the oscillations in the nℓ cross section is 90° out-of-phase with respect to the $n(\ell \pm 1)$ cross section [9]. Therefore, in the sum over ℓ, these geometric oscillations largely cancel one another so that the appearance of the second collective resonance is evident. In other words, this second collective resonance contributes to each of the subshell cross sections, but it is mostly masked by the confinement oscillations. Only in the total cross section, where the confinement oscillations largely cancel out, does it emerge clearly. This is shown in the bottom panel of figure 3 which displays total π cross sections, $\sum_\ell \sigma_{2\ell}$. The sum kills the oscillations to uncover the plasmon-induced enhancement in the TDLDA result at 38 eV. Evidently, therefore, a mechanism of constructive superpositions of independent subshell cross sections is responsible for building the plasmon resonances in the total π ionization cross section. While the phenomenon is very clear for the 16.5 eV resonance, for the 38 eV resonance the effect is somewhat masked.

Figure 4 delineates this phenomenon of constructive build-up for five outer σ subshells: 1 l, 1 k, 1 j, 1 i and 1 h. A resonant feature maximizes for each subshell just at 38 eV and accumulates the strength to create a large resonance in the total σ TDLDA cross section. Comparison between the LDA and TDLDA results for total π and total σ cross sections also suggests a stronger relative enhancement in σ than in π

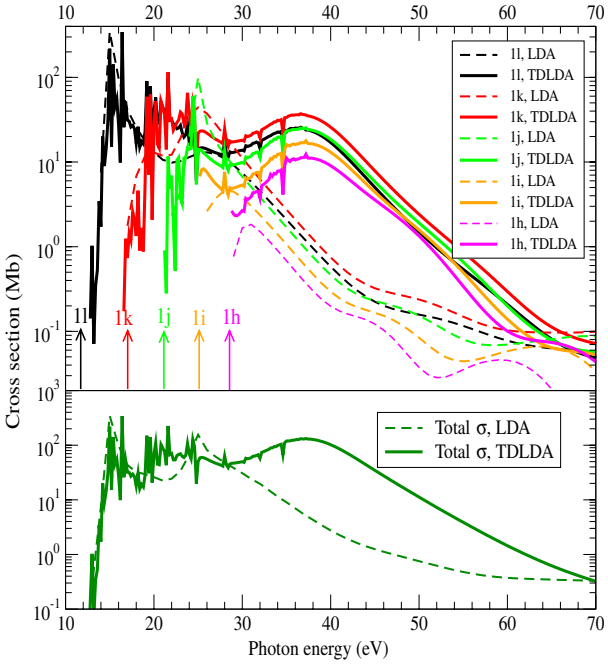

Figure 4. Upper panel: LDA and TDLDA cross sections for the five outer σ subshells of C_{60}. Lower panel: LDA and TDLDA total photoionization cross sections for all σ electrons of C_{60}.

from the 38 eV plasmon; the value of the ratio of TDLDA and LDA cross sections for total σ at 38 eV is roughly 30, while that for total π is about 6.5. This stronger influence of the high-energy plasmon on σ subshells dominates the effects of geometric oscillations on the TDLDA 1ℓ results. However, it is noteworthy that the outermost 1 l channel, that opens at 11.5 eV, well below the giant plasmon resonance, hardly contributes to this 16.5 eV resonance, as seen in figure 4. In summary, therefore, over the entire plasmon-active energy region the π ionization cross section contribution dominates the 16.5 eV resonance, while both π and σ cross sections jointly contribute (roughly equally) to the 38 eV resonance.

The general phenomenon can be characterized by the Fano formalism [32] to perturbatively include the effects of interchannel coupling upon the final state wavefunction of each of the perturbed dipole matrix elements, $M_{n\ell}(E)$:

$$M_{n\ell}(E) = D_{n\ell}(E) + \sum_{n'\ell'\neq n\ell} \int \mathrm{d}E' \frac{\langle \psi_{n'\ell'}(E') \left| \frac{1}{|\mathbf{r}_{n\ell} - \mathbf{r}_{n'\ell'}|} \right| \psi_{n\ell}(E) \rangle}{E - E'} D_{n'\ell'}(E') \tag{17}$$

where $D_{n\ell}$ is the unperturbed (LDA) $n\ell$ matrix element, $\psi_{n\ell}(E)$'s are the unperturbed final continuum state wavefunctions of the single-electron channels and the sum is over all of the photoionization channels except the $n\ell$ channel. The matrix element within the integral of equation (17) is known as the interchannel coupling matrix element; the fact that each of the $n\ell$ initial state orbital overlaps strongly with all other C_{60} orbitals, as seen in figure 1, ensures that these interchannel coupling matrix elements will be strong. Further, the existence of both low- and high-energy plasmons at exactly the same energies for all the subshells (figures 3 and 4) implies the various dipole matrix elements are 'in-phase' over the two energy regions, and hence the various terms in the sum in equation (17) will add up *coherently*, leading to the dramatic increase. Therefore, a phase-coherent interchannel coupling phenomenology must be responsible for the resonant enhancement in each subshell cross section.

3.3. Comparison with experiment

In figure 5 the calculated total cross section is compared with the experimental measurements [1, 16]. As can be seen, the experimental data produce a smoother curve without any evidence of autoionizing resonances, which exists in the theoretical TDLDA result. In the context of the photoabsorption of metal clusters, studies indicate two effects from the finite temperature of the experimental sample: (i) coupling of the electronic motion with the temperature-induced vibration modes of the ion core [33], and (ii) significant fluctuation of the cluster shape around the shape at absolute zero [34, 35]. In addition, the jellium model potential used in the present calculation over-delocalizes the valence electrons. Owing to this, the calculated wavefunctions of the valence electrons are too diffuse, compared to the true wavefunctions, i.e., the calculated wavefunctions are spread out over too large a distance. Since the autoionization rate involves a matrix element of $1/r_{12}$, the more spread out wavefunctions translate to a value of the matrix element of $1/r_{12}$ that is too small. As a consequence, the model predicts autoionization rates that are too small, thereby producing widths that are too narrow, as seen in the comparison with experiment.

In order to account for the difficulties of autoionization rates that are too small, and these additional decay channels, the theoretical cross section is convoluted with a small width. This is effected by introducing a Lorentzian of 0.4 eV width into equation (12) in place of the delta function. The convoluted result, also shown in figure 5, exhibits good qualitative agreement with the data, better than the un-convoluted result; in particular, the narrow autoionizing resonances have vanished in the convoluted result. In fact, they are not gone, and their oscillator strength is still there. Only with the extra width that was added, they no longer show up as spikes. There still, however, remain significant disagreements in the details of the result, as discussed below.

The theoretical plasmon resonance energies are somewhat below experiment. The theoretical peak at 16.5 eV for the low-energy resonance occurs at 3.5 eV below the experimental position of 20 eV. The redshift occurring for the high-energy resonance is somewhat less—about 2.0 eV. In addition, there are two very significant discrepancies. Firstly, as seen in figure 5, the nonresonant background experimental cross sections is about three times larger than what theory (with the extra width) predicts. Secondly, the theoretical resonances are narrower than those of the corresponding measured profiles; for example, the width of the low-energy plasmon that our calculation yields is about 3.5 eV, as opposed to the

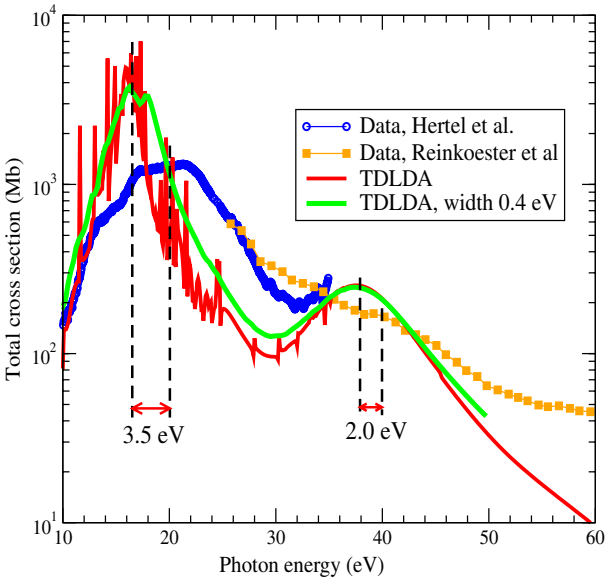

Figure 5. TDLDA total photoionization cross section of C_{60} compared with the experimental data of Hertel *et al* [1] and Reincöster *et al* [16]. In a separate curve, the TDLDA result with 0.4 eV Lorentzian width is also shown. The separations between the theoretically determined and measured plasmon positions are indicated.

experimental width of 10 eV reported in [1]. However, what is remarkable is that over the entire plasmon region, from threshold up to 90 eV photon energy, the total oscillator strength predicted by theory is ∼175, which is very close to the oscillator strength sum evaluated using the experimental data. The implication is that, although the theoretical resonances are higher and narrower than their experimental counterparts, the total oscillator strength in each plasmon agrees rather well with experiment.

In a jellium model, the plasmon resonances decay via the degenerate single-electron channels. The absence of any other decay mechanism leads to the fact that the major portion of the oscillator strength available to the system is exhausted by the collective resonances, keeping the non-resonant background of the cross section rather low. The real system, however, cannot be treated as being composed of 240 completely delocalized valence electrons, as in the jellium model. There would be effects from the independent local ion sites, at least for relatively more tightly bound electrons, that would somewhat reduce the degree of electronic delocalization. Some probability of ionization from this local ion sites, positioned appropriately, will therefore exist. These new channels, not present in a jellium model, will provide additional decay paths for the plasmon in a real system, thus increasing their widths as seen in the experimental data. Photoelectron emission from this local ion sites may also be responsible for the large non-resonant background value in the experimental cross sections.

Furthermore, an approximate effect of inclusion of ion sites is the existence of some kind of average restoring force to the collective motion of the electrons. From a classical perspective the consequence of this additional restoring force is an up-shift of the oscillation frequency of the plasmons from their jellium model values. Also, since for a classical oscillator the force is proportional to the square of the frequency, this shift must be quadratic in nature. Indeed, $\sqrt{(38)^2 + [(20)^2 - (16.5)^2]} = 39.6$ eV, which is very close to the experimental position of 40 eV of the high-energy plasmon resonance.

4. Conclusion

The photoionization cross section of C_{60} is calculated in a TDLDA framework that includes all essential many-body correlations to treat the motion of 240 delocalized electrons. The carbon ion core is represented by a spherical jellium shell. The total cross section result reveals two plasmons characteristic to the C_{60} photoionization cross section. To acquire detailed insight in the mechanism that creates these resonances, the individual π and σ subshell cross sections are also analysed. A phase-coherent interchannel coupling mechanism is found to cause enhancements in subshell cross sections. It is seen that the constructive superposition of enhancements from various subshells exactly at the energies of plasmon excitations generates the collective resonances.

The results are also compared with the available measurements. While good qualitative agreement is found, there remain significant discrepancies in quantitative comparison. These discrepancies are attributed to the known over-delocalization of electrons intrinsic to a jellium model. It is inferred that further improvement can only be accomplished by going beyond the jellium framework to treat the ions appropriately placed depending on the molecular symmetry. Non-jellium molecular orbital-type density functional calculations [36], can, in principle, be more accurate. Nevertheless, as shown earlier [10], the jellium model prediction agrees reasonably with these results, as well as with the experimental data, for the ratio of the HOMO and HOMO-1 cross sections of C_{60}. However, the inclusion of many-body effects for a dynamical process is far more conveniently adoptable in a jellium framework. Indeed, no time-dependent calculation has so far been done in a framework of the type of [36]. To this end, therefore, our results represent the best that a jellium model can produce and may indicate that the jellium result augmented with appropriate extra width to include an average effect of all omitted decay channels may provide an improved comparison with the experiment.

Finally, note that a wealth of detail in the subshell cross sections washes out in the total cross section, e.g., the confinement oscillations in the vicinity of the higher-energy plasmon. Thus, experimental photoelectron studies of the photoionization of C_{60} would be most valuable.

Acknowledgments

The work is supported partly by the NSF and the DOE, Basic Energy Sciences. MEM and HSC also acknowledge the Max-Planck-Institut für Physik Komplexer Systeme, Dresden, Germany, where most of the calculations were performed.

References

[1] Hertel I V, Steger H, de Vries J, Weisser B, Menzel C, Kamke B and Kamke W 1992 *Phys. Rev. Lett.* **68** 784
[2] Bertsch G F, Bulgac A, Tománek D and Wang Y 1991 *Phys. Rev. Lett.* **67** 2690
[3] Tománek D and Schluter M A 1991 *Phys. Rev. Lett.* **67** 2331
[4] Rubio A, Alonso J A and López J M 1993 *Physica* B **183** 247
[5] Alasia F, Broglia R A, Roman H E, Serra L, Colo G and Pacheco J M 1994 *J. Phys. B: At. Mol. Opt. Phys.* **27** L643
[6] Puska M J and Nieminen R M 1993 *Phys. Rev.* A **47** 1181
[7] Wendin G and Wästberg B 1993 *Phys. Rev.* B **48** 14764
[8] Scully S W J *et al* 2005 *Phys. Rev. Lett.* **94** 065503
[9] Frank O and Rost J M 1997 *Chem. Phys. Lett.* **271** 367
[10] Rüdel A, Hentges R, Becker U, Chakraborty H S, Madjet M E and Rost J M 2002 *Phys. Rev. Lett.* **89** 125503
[11] Korica S, Rolles D, Reinköster A, Langer B, Viefhaus J, Cvejanovic S and Becker U 2005 *Phys. Rev.* A **71** 013203
[12] Ivanov V K, Kashenock G Yu, Polozkov R G and Solov'yov A V 2001 *J. Phys. B: At. Mol. Opt. Phys.* **34** L669
[13] Polozkov R G, Ivanov V K and Solov'yov A V 2005 *J. Phys. B: At. Mol. Opt. Phys.* **38** 4341
[14] Korol A V and Solov'yov A V 2007 *Phys. Rev. Lett.* **98** 179601
[15] Scully S W J *et al* 2007 *Phys. Rev. Lett.* **98** 179602
[16] Reinköster A, Korica S, Pruemper G, Viefhaus J, Godehausen K, Schwarzkopf O, Mast M and Becker U 2004 *J. Phys. B: At. Mol. Opt. Phys.* **37** 2135
[17] Madjet M E and Hervieux P A 1999 *Eur. Phys. J.* D **9** 217
[18] Madjet M E, Chakraborty H S and Rost J M 2001 *J. Phys. B: At. Mol. Opt. Phys.* **34** L345
[19] Gunnerson O and Lundqvist B 1976 *Phys. Rev.* B **13** 4274
[20] Vos M, Canney S A, McCarthy I E, Utteridge S, Michalewicz M T and Weigold E 1997 *Phys. Rev.* B **56** 1309
[21] Troullier N and Martins J L 1992 *Phys. Rev.* B **46** 1754
[22] Weaver J H, Martins J L, Komeda T, Chen Y, Ohno T R, Kroll G H and Troullier N 1991 *Phys. Rev. Lett.* **66** 1741
[23] Martins J L, Troullier N and Weaver J H 1991 *Chem. Phys. Lett.* **180** 457
[24] Antoine R, Rayane D, Benichou E, Dugourd Ph and Broyer M 2000 *Eur. Phys.* D **12** 147
[25] Ekardt W 1985 *Phys. Rev.* B **31** 6360
[26] Zangwill A and Soven P 1980 *Phys. Rev.* A **21** 1561
[27] Hervieux P-A, Madjet M E and Benali H 2002 *Phys. Rev.* A **65** 023202
[28] Bertsch G F 1990 *Comput. Phys. Commun.* **60** 247
[29] Bethe H A and Salpeter E E 1958 *Quantum Mechanics of One- and Two-Electron Atoms* (Berlin: Springer) p 255
[30] Puska M J, Nieminen R M and Manninen M 1985 *Phys. Rev.* B **31** 3486
[31] Lambin Ph, Lucas A A and Vigneron J-P 1992 *Phys. Rev.* B **46** 1794
[32] Fano U 1961 *Phys. Rev.* A **124** 1866
[33] Bertsch G F and Tománek D 1989 *Phys. Rev.* B **40** 2749
[34] Penzar Z, Ekardt W and Rubio A 1990 *Phys. Rev.* B **42** 5040
[35] Pacheco J M and Broglia R A 1989 *Phys. Rev. Lett.* **62** 1400
[36] Decleva P, Furlan S, Fronzoni G and Stener M 2001 *Chem. Phys. Lett.* **348** 363